The formation and phase transition of vortex domain structures in ferroelectric nanodots: First-principles-based simulations

J. Y. Liu, W. J. Chen, B. Wang, and Yue Zheng

Citation: Journal of Applied Physics **114**, 044101 (2013); doi: 10.1063/1.4815963

JOURNAL OF APPLIED PHYSICS **114**, 044101 (2013)

The formation and phase transition of vortex domain structures in ferroelectric nanodots: First-principles-based simulations

J. Y. Liu, W. J. Chen, B. Wang,[a] and Yue Zheng[a]
State Key Laboratory of Optoelectronic Materials and Technologies, School of Physics and Engineering, Sun Yat-sen University, 510275 Guangzhou, China and Micro&Nano Physics and Mechanics Research Laboratory, School of Physics and Engineering, Sun Yat-sen University, 510275 Guangzhou, China

(Received 4 June 2013; accepted 1 July 2013; published online 22 July 2013)

Effects of size and hydrostatic pressure on the formation of vortex domain structures (VDSs) in ferroelectric nanodots under the open circuit condition have been simulated using the effective Hamiltonian method. Our calculations indicate promising controllability of VDS in the nanodots. Interestingly, it is found that the VDS holds rhombohedral at various sizes and pressures. Furthermore, the paraelectric-ferrotoroidic phase transition temperature (T_{FD}) is very sensitive to size and pressure, manifesting with near linear relationships in most investigated range. At high pressure range, we found that the T_{FD}-pressure curves become nonlinear. It indicates that the traditional Landau potentials with polarization-strain coupling term up to $\sim P\varepsilon^2$ are not sufficient to describe the high pressure effect and the expansion coefficients should be modified as pressure dependent. © *2013 AIP Publishing LLC*. [http://dx.doi.org/10.1063/1.4815963]

I. INTRODUCTION

Over the past decades, ferroelectric materials have attracted an enormous amount of attentions because of their special physical properties, which imply great potential value in device applications, including ferroelectric random access memories (FERAMs),[1] sensors,[2] transducers,[3] actuators,[4] etc. Nowadays, with the trend of miniaturization and integration of devices and the improvement of material preparation technology, ferroelectric nanostructures (FNs) are expected to play important roles in future functional devices.[5] FNs usually present quite different properties from those of their bulk counterparts due to the size, surface, and interface effects. Actually, lots of studies have been done to figure out the unique properties, e.g., the ferroelectric size effect that may exist in low dimensional FE materials in FNs.[6–8] Recently, several works have reported that low dimensional FNs in small size can exhibit vortex domain structures (VDSs),[9,10] which are similar to those in magnetic nanostructures.[11–13] This finding opens exciting opportunities for designing novel functional devices. For example, a ferroelectric nanodot with VDS can be used as a memory cell by controlling the vortex chirality, which enables ultra-high storage density due to the small size of nanodot.[9] Other examples reside in the novel characteristics of VDS to external fields, e.g., the enhanced electromechanical response found in ferroelectric nanowires due to vortex formation induced by modulated electric field,[14] facilitating the piezoelectric applications when devices are miniaturized to nanoscale. Therefore, the controllability of VDSs, which is the key to promising applications, is a very important topic.

The low dimensional FNs are considered to form toroidal order of polarization configuration to reduce the strong depolarizing field caused by the uncompensated charges at the surface. Thus, the formation of VDS is supposed to strongly depend on effects of many factors like size and boundary conditions of the nanostructures. In fact, the mechanism of forming VDS in FNs and novel ways to control it, e.g., effects caused by screening of depolarizing field,[15,16] applied stress,[17] electric field,[18] etc., have been theoretically investigated by various approaches, such as thermodynamic modeling, first-principle calculations, and first-principles-based atomic level methods. Experimentally, the characteristics of the VDS have been detected by piezoresponse force microscopy (PFM) or other methods in several works.[19,20] Nevertheless, despite all the intense efforts above, research on VDS in FNs is still in its infancy, and many problems remain unsolved both in theory and experiment. Discovering regularity of VDS formations is crucial for future applications.

Effect of hydrostatic pressure on the phase transition and properties of ferroelectric materials has been a long investigated topic for many decades, which is important to understand the nature of ferroelectrics. Experimenters have a lot of efforts to reveal the dependence of the properties of ferroelectrics on pressure and temperature.[21,22] However, due to the difficulty of high pressure experiments, not much substantial advances were achieved until the great development of the high pressure apparatus and numerical simulation techniques. Particularly, using a first-principles-derived method, Zhong *et al.*[23] calculated the temperature-pressure phase diagram of bulk $\mathrm{BaTiO_3}$. Similar results were later obtained by Ishidate *et al.*[24] in experiment.

Despite the well-known researches about hydrostatic pressure effect on bulk ferroelectrics, the formation of VDS in FNs at various pressures has not yet been investigated and discussed. Such kind of study should be instructive in both fundamental research and application of VDS. In this letter,

---

[a] Authors to whom correspondence should be addressed. Electronic addresses: zhengy35@mail.sysu.edu.cn and wangbiao@mail.sysu.edu.cn

a first-principles-derived effective Hamiltonian approach[23] coupled with Monte Carlo simulations is used to investigate the temperature, size, and hydrostatic pressure dependence of the formation of VDSs in $BaTiO_3$ nanodots. The forming behaviors of VDS at various sizes and pressures are presented, respectively. Then, the size and pressure effects are summarized in the end, and the mechanism of which is discussed on the basis of the results.

II. THE EFFECTIVE HAMILTONIAN MODEL

In following simulations, we adopt the effective Hamiltonian proposed for ferroelectric materials.[23] The total energy can be written as a sum of five energies

$$\begin{aligned} &E^{\mathrm{tot}}(\{\mathbf{u}_i\},\{\mathbf{v}_i\},\{\eta_{H,l}\}) \\ &\quad = E^{\mathrm{self}}(\{\mathbf{u}_i\}) + E^{\mathrm{dpl}}(\{\mathbf{u}_i\}) + E^{\mathrm{short}}(\{\mathbf{u}_i\}) \\ &\qquad + E^{\mathrm{elas}}(\{\mathbf{v}_i\},\{\eta_{H,l}\}) + E^{\mathrm{int}}(\{\mathbf{u}_i\},\{\mathbf{v}_i\},\{\eta_{H,l}\}), \end{aligned} \tag{1}$$

where $\mathbf{u}_i$ is the local soft-mode amplitude vector in unit cell i, $\{\mathbf{v}_i\}$ are the local dimensionless displacements related to the inhomogeneous strain, and $\eta_{H,l}$ is the homogeneous strain tensor. E^{self} $(\{\mathbf{u}_i\})$, E^{dpl} $(\{\mathbf{u}_i\})$, E^{short} $(\{\mathbf{u}_i\})$, E^{elas} $(\{\mathbf{v}_i\}$, $\{\eta_{H,l}\})$, and E^{int} $(\{\mathbf{u}_i\}$, $\{\mathbf{v}_i\}$, $\{\eta_{H,l}\})$ are local mode self-energy, long-range dipole-dipole coupling, short-range interaction between local modes, elastic energy, and the interaction between the local modes and local strain, respectively.

The local-mode self-energy E^{self} $(\{\mathbf{u}_i\})$ is a summation of energies of the isolated local modes of all cells

$$E^{\mathrm{self}}(\{\mathbf{u}_i\}) = \sum_i (\kappa_2 u_i^2 + \alpha u_i^4 + \gamma(u_{ix}^2 u_{iy}^2 + u_{iy}^2 u_{iz}^2 + u_{iz}^2 u_{ix}^2)), \tag{2}$$

where $u_i = |\mathbf{u}_i|$, i runs from 1 to N (N is the number of primitive cells in the nanodot), and κ_2, α, and γ are expansion parameters determined by first-principles calculations.

The long-range dipole-dipole interaction E^{dpl} $(\{\mathbf{u}_i\})$ between local modes is

$$E^{\mathrm{dpl}}(\{\mathbf{u}_i\}) = \frac{Z^{*2}}{2\varepsilon_\infty} \sum_{i,j,\alpha\beta} Q_{ij,\alpha\beta} u_{i,\alpha} u_{j,\beta}, \tag{3}$$

where ε_∞ is the optical dielectric constant, Z^* is the Born effective charge for the soft mode, α and β denote Cartesian components, and Q is treated as a constant matrix, written as $Q_{ij,\alpha\beta} = \delta_{\alpha\beta}/R_{ij}^3 - 3R_{\alpha,ij}R_{\beta,ij}/R_{ij}^5$ for nanodot. Here, $\delta_{\alpha\beta}$ is the Kronecker delta, $R_{ij} = |\mathbf{R}_{ij}|$, and $\mathbf{R}_{ij} = \mathbf{R}_i - \mathbf{R}_j$, where $\mathbf{R}_i$ labels the center site of cell i. The sum runs over the cell sites i and j that differ from each other.

The short-range interaction E^{short} $(\{\mathbf{u}_i\})$ between neighboring local modes is

$$E^{\mathrm{short}}(\{\mathbf{u}_i\}) = \frac{1}{2} \sum_{i \neq j} \sum_{\beta\alpha} J_{ij,\alpha\beta} u_{i,\alpha} u_{j,\beta}, \tag{4}$$

where $J_{ij,\alpha\beta}$ is the short-range coupling matrix, defined as a function of $\mathbf{R}_{ij}$. We take account of the short-range interaction up to third nearest neighbor, considering the fast decay of it with increasing $|\mathbf{R}_{ij}|$. The coupling matrix $J_{ij,\alpha\beta}$ can be simplified to only seven interaction parameters by symmetry.[23]

The total elastic energy can be written as a sum of two parts

$$E^{\mathrm{elas}}(\{\mathbf{v}_i\},\{\eta_{H,l}\}) = E_H^{\mathrm{elas}}(\{\eta_{H,l}\}) + E_I^{\mathrm{elas}}(\{\mathbf{v}_i\}), \tag{5}$$

where the homogeneous strain energy is

$$\begin{aligned} E_H^{\mathrm{elas}}(\{\eta_{H,l}\}) = {} & \frac{N}{2} B_{11}(\eta_{H,1}^2 + \eta_{H,2}^2 + \eta_{H,3}^2) \\ & + NB_{12}(\eta_{H,1}\eta_{H,2} + \eta_{H,2}\eta_{H,3} + \eta_{H,3}\eta_{H,1}) \\ & + \frac{N}{2} B_{44}(\eta_{H,4}^2 + \eta_{H,5}^2 + \eta_{H,6}^2), \end{aligned} \tag{6}$$

and the inhomogeneous strain energy is

$$\begin{aligned} E_I^{\mathrm{elas}}(\{\mathbf{v}_i\}) = \sum_i \{ & \gamma_{11}[v_x(\mathbf{R}_i) - v_x(\mathbf{R}_i \pm \mathbf{x})]^2 \\ & + \gamma_{12}[v_x(\mathbf{R}_i) - v_x(\mathbf{R}_i \pm \mathbf{x})][v_y(\mathbf{R}_i) - v_y(\mathbf{R}_i \pm \mathbf{y})] \\ & + \gamma_{44}[v_x(\mathbf{R}_i) - v_x(\mathbf{R}_i \pm \mathbf{y}) + v_y(\mathbf{R}_i) \\ & - v_y(\mathbf{R}_i \pm \mathbf{x})]^2 + cyclicperm.\}. \end{aligned} \tag{7}$$

Here, B_{11}, B_{12}, and B_{44} are the elastic constants, and the γ coefficients are related to them by $\gamma_{11} = B_{11}/4$, $\gamma_{12} = B_{12}/8$, and $\gamma_{44} = B_{44}/8$. $\mathbf{x} = a\hat{\mathbf{x}}$, $\mathbf{y} = a\hat{\mathbf{y}}$, $\mathbf{z} = a\hat{\mathbf{z}}$, where a is the lattice constant, and $\hat{\mathbf{x}}$, $\hat{\mathbf{y}}$, and $\hat{\mathbf{z}}$ are unit vectors.

The coupling between the elastic deformations and the local modes is

$$E^{\mathrm{int}}(\{\mathbf{u}_i\},\{\mathbf{v}_i\},\{\eta_{H,l}\}) = \frac{1}{2} \sum_i \sum_{l\alpha\beta} B_{l\alpha\beta} \eta_l(\mathbf{R}_i) u_\alpha(\mathbf{R}_i) u_\beta(\mathbf{R}_i), \tag{8}$$

where $B_{l\alpha\beta}$ are the coupling constants, and l runs from 1 to 6. Only B_{1xx}, B_{1yy}, and B_{4yz} are independent due to the result of cubic symmetry. The total strain contains two parts. $\eta_l(\mathbf{R}_i) = \eta_{H,l}(\mathbf{R}_i) + \eta_{I,l}(\mathbf{R}_i)$. The inhomogeneous strain is expressed in terms of the local displacement vectors $\{\mathbf{v}_i\}$ that have been defined.[23]

III. RESULTS AND DISCUSSIONS

In the following calculations, the $BaTiO_3$ nanodot is assumed to be BaO-terminated. The local mode is Ti-centered and the displacement is centered on Ba-sites. Compared with the Hamiltonian in Ref. 23, several adjustments are made in order to simulate $BaTiO_3$ nanodots. No periodic boundary conditions are imposed in the interaction between the local modes. The long-range dipole-dipole interaction is performed in real space.

We calculate the cubic $BaTiO_3$ nanodots with size being $na \times na \times na$, where n is the number of the five-atom unit cell along one of the coordinate directions, and $a = 7.46$a.u. is the lattice constant. In our simulations, at least 20 000 Monte Carlo sweeps are first preformed to equilibrium the system, and then up to 100 000 sweeps are used to get the statistical average for each temperature. All the simulations are quasi-static cooling process under ideal open-circuit condition, and the temperature is decreased in small steps, typically 10 K.

We first calculate a 12 × 12 × 12 $BaTiO_3$ nanodot at the pressure $p = -4.8$ GPa, which is found to be a good correction for the underestimated lattice constants introduced by local density approximation (LDA) of the first principles simulation.[23] We characterize the VDS in ferroelectric nanodot by toroidal moment,[25] defined as $\mathbf{g} = 1/(2N\upsilon)\sum_i \mathbf{r}_i \times \mathbf{p}_i$, where υ is volume of the unit cell and $\mathbf{p}_i$ is the dipole moment of cell i located by position vector $\mathbf{r}_i$. The orientation of the toroidal moment can be characterized by introducing (θ, φ), describing the angle between the toroidal moment vector and z axis and the angle between x axis and the projection of the toroidal moment vector on the x-y plane, respectively. The total polarization is calculated by $\mathbf{P} = 1/(N\upsilon)\sum_i \mathbf{p}_i$.[25] The average of the polarization magnitude of all sites, i.e., $\bar{P} = 1/(N\upsilon)\sum_i |\mathbf{p}_i|$, is also introduced to denote the paraelectric-ferrotoroidic phase transition.

A. Effect of temperature on the vortex domain structures of ferroelectric nanodot

Fig. 1 shows the simulated results of a 12 × 12 × 12 $BaTiO_3$ nanodot. It can be seen from Fig. 1(a) that the magnitude of the toroidal moment g is close to zero at high temperature. However, when the nanodot is cooling down and passes through about 270 K, g becomes nonzero and increases with the decreasing temperature, which implies that paraelectric-ferrotoroidic phase transition occurs. The three components of the toroidal moment, $|g_x|$, $|g_y|$, and $|g_z|$, coincide well with each other during most of the cooling-down process, expect that minor differences can be found at low temperature. Moreover, the average of polarization magnitude of all sites $\bar{P}$ is nonzero when the temperature is lower than about 270 K, similar to the variation in toroidal moment shown in Fig. 1(a), whereas the total polarization remains nearly null at all temperatures (see Fig. 1(b)). The direction of the toroidal moment (θ, φ) is depicted in Fig. 1(c). All these results indicate that a rhombohedral VDS along [111] is formed in the nanodot. This is further verified by the morphologies of the stable domain pattern plotted in Fig. 1(d). The rhombohedral VDS is consistent with the ground state of bulk $BaTiO_3$ which is in rhombohedral phase at low temperature. The absence of tetragonal and orthorhombic VDSs but only rhombohedral VDS is similar to previous studies using effective Hamiltonian simulation and phase field simulation.[16,25]

B. Size effects on the vortex domain structures of ferroelectric nanodot

Based on the characteristics shown in Fig. 1, we extend our simulations at various sizes denoted by n, with n ranging from 6 to 16, to investigate the size effect on the formation of the VDS. The simulations are still under the hydrostatic pressure −4.8 GPa. The simulated results are shown in Fig. 2. We can see from Fig. 2(a) that the toroidal moment of different sizes have similar change tendency during the cooling-down process of temperature. At a given temperature, it increases with the increase of the size obviously. At the same time, the paraelectric-ferrotoroidic phase transition temperature (T_{FD}) also increases with the size increasing. As the size deceases, the phase transition becomes less abrupt. Note that in our simulation, we did not incorporate the surface term[10] in the effective Hamiltonian, which may have impact on the phase transition temperature. According to the morphologies of the VDS at 0 K plotted in Fig. 2(b), it seems that the direction of the toroidal moment in cubic $BaTiO_3$ hardly changes with size. Especially, it is worth mentioned that for the 16 × 16 × 16 $BaTiO_3$ nanodot, when the temperature is cooled down to about 50 K, a slightly decrease of the magnitude of toroidal moment is found. Correspondingly,

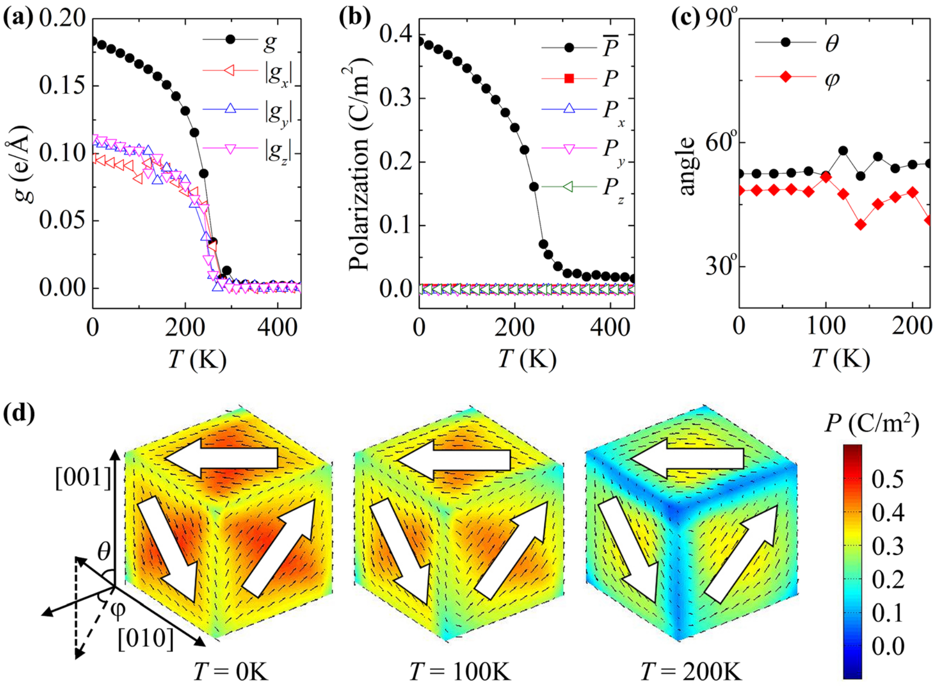

FIG. 1. Simulated results of a 12 × 12 × 12 $BaTiO_3$ nanodot under ideal open-circuit condition at $p = -4.8$GPa. The variation of (a) magnitude of toroidal moment, (b) polarization, (c) direction of toroidal moment, and (d) the vortex domain structures with temperature. All vortex domain patterns in the figures behind are shown with the same color bar scale.

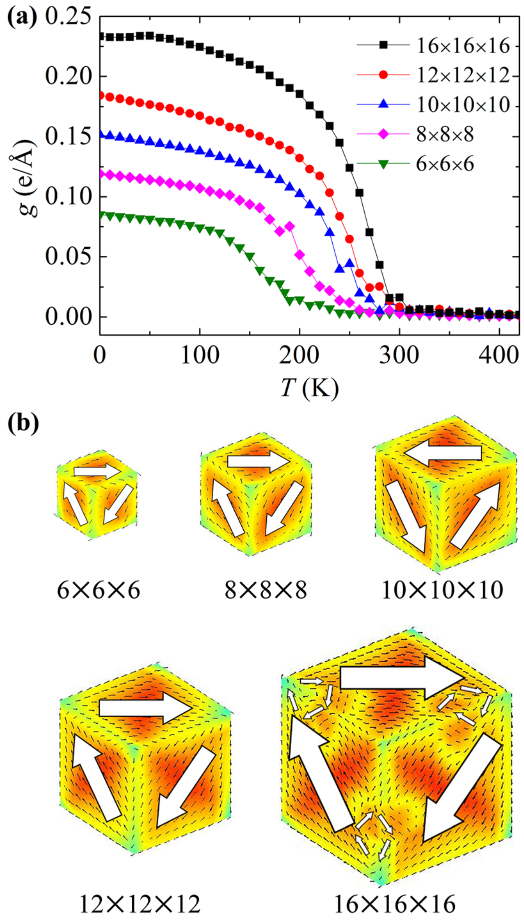

FIG. 2. (a) The toroidal moments of nanodots with different sizes as a function of temperature and (b) vortex domain patterns of some selected sizes at $T = 0$ K.

some small additional vortex patterns arise around the midpoint of the edges of the cubic nanodot (see Fig. 2(b)).

C. Effects of pressure on the vortex domain structure of ferroelectric nanodot

As mentioned above, hydrostatic pressure, which is reported to be crucial in the phase transition of ferroelectrics, is expected to play an important role in the formation and controllability of the VDS in BaTiO$_3$ nanodots. To investigate this, we further simulate the $12 \times 12 \times 12$ BaTiO$_3$ nanodot with the pressure ranging from -7 GPa to 9 GPa. Simulated result (Fig. 3(a)) shows that both T_{FD} and g decrease significantly with the increase of hydrostatic pressure. More importantly, the T_{FD} can be shifted within a wide range by adjusting hydrostatic pressure. Application of a positive hydrostatic pressure (compared with $p = -4.8$ GPa which is considered to be theoretical zero pressure) depresses the formation of the VDS. When the pressure reaches as high as 7 GPa, no stable VDS is found at all temperatures. Interestingly, the vortex patterns remain single domain and rhombohedral at different pressures except that a different pattern ($|g_x|>|g_z|>|g_y|$) is captured at $T = 0$ K with $p = 7$ GPa, which is actually quite unstable and near paraelectric state as shown in Fig. 3(b). No other ferroelectric phase or polarization pattern is found. The full phase

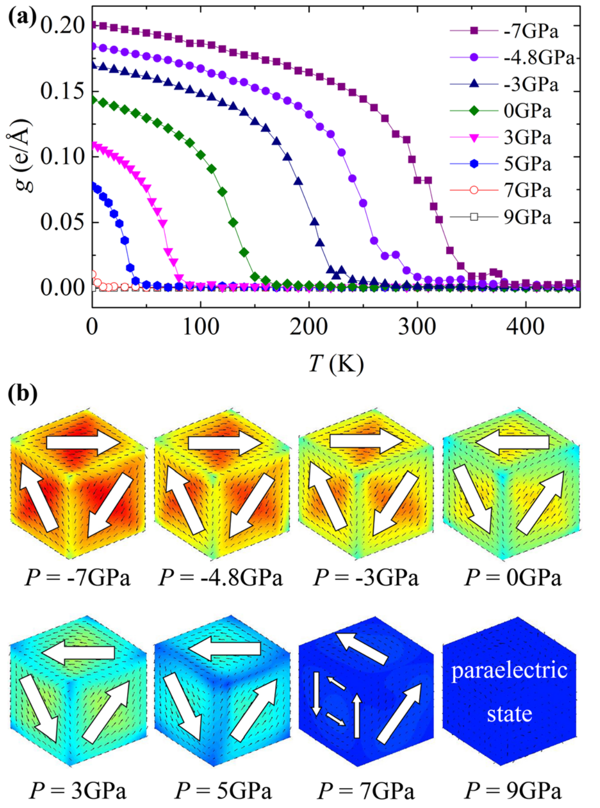

FIG. 3. (a) Simulated toroidal moments of a nanodot under different pressures as a function of temperature and (b) the vortex domain patterns at some selected pressures at $T = 0$ K.

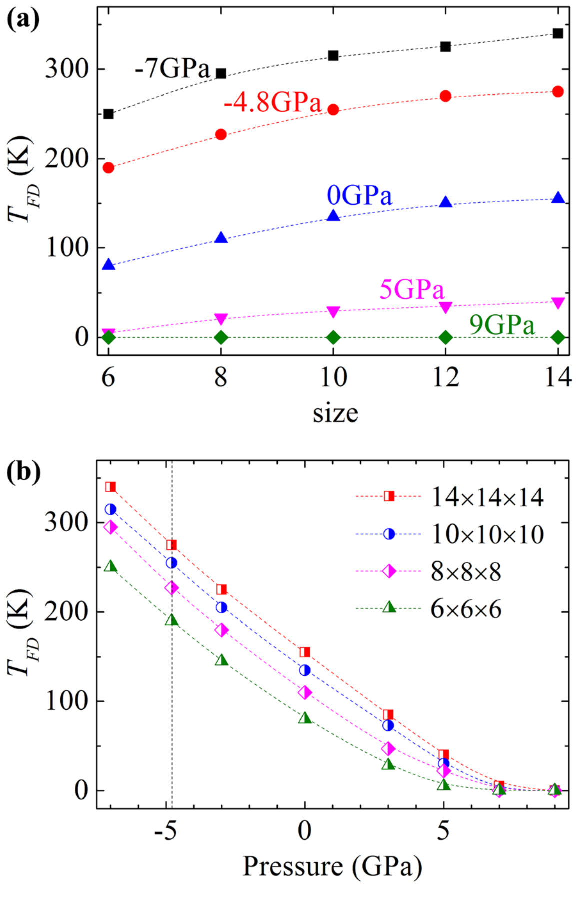

FIG. 4. The calculated functional relation between (a) T_{FD} and size at different pressures and (b) T_{FD} and pressure at various sizes.

transition sequence present in the bulk $BaTiO_3$ cannot be induced by pressure effect in our simulations here.

D. The paraelectric-ferrotoroidic phase transition temperature determined by effects of size and pressure

To fully investigate the size and pressure effects, we further extend our simulations to various sizes and hydrostatic pressures, and the results are summarized in Fig. 4. Fig. 4(a) shows the T_{FD} as a function of the size of cubic nanodots. The T_{FD} in $BaTiO_3$ nanodots is a little lower than the ferroelectric transition temperature in their bulk counterparts and it increases with size slowly. The near linear relation between the T_{FD} and pressure is obtained and depicted in Fig. 4(b), which demonstrates a fast reduction of the T_{FD} with the increase of the pressure. Particularly, the slope (dT_c/dp) remains nearly unchanged at low pressures, whereas it decreases at high pressures. Note that this nonlinear behavior is not expected in phase field simulation based on the traditional Landau potentials,[26] which describe the coupling effect between polarization and strain by incorporating a coupling term $\sim P\varepsilon^2$, with all the expansion coefficients being independent of pressure. As we know, the pressure effect is equivalent to applying an isotropic strain, and this strain leads to a renormalization of the phase transition temperature as $\Delta T_c \propto \varepsilon \propto p$. Accordingly, T_{FD} should be also linearly proportional to hydrostatic pressure. The contradiction between the two approaches indicates that the traditional Landau potentials only with polarization-strain coupling term $\sim P\varepsilon^2$ are not sufficient to describe the high pressure effect. Although a coupling term $\sim P\varepsilon^2$ is sufficient for most purposes, such as the formation of VDS in $BaTiO_3$ dots in low pressure conditions, a modification of the expansion coefficients to be pressure dependent should become essential when it comes to high pressure conditions.

IV. CONCLUSIONS

In summary, effects of size and hydrostatic pressure on the formation of VDSs in $BaTiO_3$ nanodots at open-circuit condition have been investigated using the effective Hamiltonian method. Our study indicates promising controllability of VDS of the nanodots by size and pressure. Interestingly, it is found that the VDS holds rhombohedral at various sizes and pressures. Furthermore, the paraelectric-ferrotoroidic phase transition temperature of the nanodot is found very sensitive to size and pressure, manifesting near linear relationships in most investigated range. At high pressure range, we found that the T_{FD}-pressure curves become nonlinear. This indicates that the traditional Landau thermodynamic potentials with polarization-strain coupling term up to $\sim P\varepsilon^2$ are not sufficient to describe the high pressure effect and the expansion coefficients should be modified as pressure dependent. The results also throw light on the actual designing of functional devices, such as pressure transducer.

ACKNOWLEDGMENTS

The authors gratefully acknowledge the financial support of NSFC (Nos. 10902128, 10732100, 50802026, 10972239). Y. Zheng also thanks support by the Fundamental Research Funds for the Central Universities, NCET in University, Research Fund for the Doctoral Program of Higher Education, and Fok Ying Tung Foundation, Science and Technology Innovation Project of Guangdong Provincial Education Department and Guangdong Natural Science Funds for Distinguished Young Scholar.

[1] O. Auciello, J. F. Scott, and R. Ramesh, Phys. Today **51**(7), 22 (1998).
[2] T. Chen and J. F. Scott, Integr. Ferroelectr. **3**, 69 (1993).
[3] S. Mathews, R. Ramesh, T. Venkatesan, and J. Benedetto, Science **276**, 238 (1997).
[4] S.-E. Park and T. R. Shrout, J. Appl. Phys. **82**, 1804 (1997).
[5] J. F. Scott, Science **315**, 954 (2007).
[6] Y. Zheng, W. J. Chen, X. Luo, B. Wang, and C. H. Woo, Acta. Mater. **60**, 1857 (2012); Y. Zheng and C. H. Woo, Nanotechnology **20**, 075401 (2009).
[7] I. Ponomareva, L. Bellaiche, and R. Resta, Phys. Rev. Lett. **99**, 227601 (2007).
[8] J. E. Spanier, A. M. Kolpak, J. J. Urban, I. Grinberg, L. Ouyang, W. S. Yun, A. M. Rappe, and H. Park, Nano Lett. **6**, 735 (2006).
[9] I. I. Naumov, L. Bellaiche, and H. Fu, Nature **432**, 737 (2004).
[10] H. Fu and L. Bellaiche, Phys. Rev. Lett. **91**, 257601 (2003).
[11] C. Kittel, Phys. Rev. **70**, 965 (1946).
[12] T. Shinjo, T. Okuno, R. Hassdorf, K. Shigeto, and T. Ono, Science **289**, 930 (2000).
[13] A. Wachowiak, J. Wiebe, M. Bode, O. Pietzsch, M. Morgenstern, and R. Wiesendanger, Science **298**, 577 (2002).
[14] X. Fu, I. I. Naumov, and H. Fu, Nano Lett. **13**, 491 (2013).
[15] I. Ponomareva, I. I. Naumov, and L. Bellaiche, Phys. Rev. B **72**, 214118 (2005).
[16] C. M. Wu, W. J. Chen, D. C. Ma, C. H. Woo, and Y. Zheng, J. Appl. Phys. **112**, 104108 (2012).
[17] W. J. Chen, Y. Zheng, and B. Wang, Sci. Rep. **2**, 796 (2012); W. J. Chen, Y. Zheng, and B. Wang, Appl. Phys. Lett. **100**, 062901 (2012).
[18] I. I. Naumov and H. Fu, Phys. Rev. Lett. **101**, 197601 (2008).
[19] B. J. Rodriguez, X. S. Gao, L. F. Liu, W. Lee, I. Naumov, A. M. Bratkovsky, D. Hesse, and M. Alexe, Nano Lett. **9**, 1127 (2009).
[20] A. Gruverman, D. Wu, H.-J. Fan, I. Vrejoiu, M. Alexe, R. J. Harrison, and J. F. Scott, J. Phys.: Condens. Matter **20**, 342201 (2008).
[21] G. A. Samara, Phys. Rev. **151**, 378 (1966).
[22] D. L. Decker and Y. X. Zhao, Phys. Rev. B. **39**, 2432 (1989).
[23] W. Zhong, D. Vanderbilt, and K. M. Rabe, Phys. Rev. B **52**, 6301 (1995).
[24] T. Ishidate, S. Abe, H. Takahashi, and N. Môri, Phys. Rev. Lett. **78**, 2397 (1997).
[25] S. Prosandeev, I. Ponomareva, I. Naumov, I. Kornev, and L. Bellaiche, J. Phys.: Condens. Matter **20**, 193201 (2008).
[26] A. F. Devonshire, Philos. Mag. **40**, 1040 (1949).